Enhancement of correlated photon-pair generation from a positive-negative index material heterostructure

Shaozhi Wei, Yunxia Dong, Haibo Wang, and Xiangdong Zhang

Department of Physics, Beijing Normal University, Beijing 100875, China

The generation efficiency of correlated photon pairs from a positive-negative index material heterostructure has been investigated by using a rigorous quantum model of spontaneous parametric down-conversion. The mean number of output photon pairs and the signal-field energy spectrum have been calculated. It is shown that the strong confinements of both the pump and signal fields around the resonance state result in a giant enhancement of the correlated photon-pair generation. The generation rate of the correlated photon pair can be improved by several orders of magnitude in the present structure in comparison with those in the corresponding conventional resonant cavity. This means that the present structure can be applied as a highly efficient potential source for entangled photon pairs.

I. INTRODUCTION

During the past few years, there has been a great deal of interest in studying how to produce entangled photon pairs, because it is an essential resource that must be freely available for implementing many of the novel functions of quantum-information processing [1,2]. Many methods to produce such a resource have been developed [1–12]. A popular approach to generating entangled pairs of photons is based on the nonlinear process of parametric down-conversion in naturally birefringent nonlinear crystals such as β-barium borate (BBO) [3]. The other mechanisms, such as using quasi-phase-matching in photonic crystals and periodically poled materials, have also been proposed [4–12].

Recently, negative index materials (NIMs) have attracted a great deal of attention from both theoretical and experimental sides [13–21]. These materials, which are characterized by simultaneous negative permittivity and permeability, possess a number of unusual electromagnetic effects [13–21]. The characteristic of single and coupled cavities made of positive index material (PIM) sandwiched between two NIMs has also been analyzed [21]. It is found that the nonlinear conversion efficiency can be improved greatly by such a system in comparison with that in the conventional resonant cavity [21]. It is natural to ask whether or not the system possesses some advantages in the generation of correlated photon states.

Motivated by such a problem, in this paper we will investigate the generation of correlated photon pairs from a positive-negative index material heterostructure. Our studies are based on the quantum theory of spontaneous parametric down-conversion. We first extend the rigorous quantum model, which has been developed in Ref. [8] for the one-dimensional dielectric photonic crystal, to the multilayer structures containing the NIMs. The two-photon amplitude and the generation rate for the correlated photon pairs in the structure will be studied in detail. The rest of the paper is organized as follows. In Sec. II, we summarize the theory and method for the generation of correlated photon pairs in the multilayer structures containing the NIMs. The numerical results and discussion are described in Sec. III. A conclusion is given in Sec. IV.

II. THEORY

We consider a cavity consisting of a positive index material sandwiched between two negative index materials (NIM-PIM-NIM). The electric and magnetic responses of the NIM are modeled with a lossy Drude model [20,21]:

$$\varepsilon(\tilde{\omega}) = 1 - \frac{1}{\tilde{\omega}(\tilde{\omega} + i\tilde{\gamma}_e)}, \quad \mu(\tilde{\omega}) = 1 - \frac{(\omega_{pm}/\omega_{pe})^2}{\tilde{\omega}(\tilde{\omega} + i\tilde{\gamma}_m)}, \quad (1)$$

Where $\tilde{\omega} = \omega/\omega_{pe}$ is the normalized frequency, ω_{pe} and ω_{pm} are electric and magnetic plasma frequency, respectively. $\tilde{\gamma}_e = \gamma_e/\omega_{pe}$ and $\tilde{\gamma}_m = \gamma_m/\omega_{pe}$ are the electric and magnetic loss terms normalized with respect to the electric plasma frequency. The middle layer is nonlinear materials such as semiconductors with high quadratic nonlinear susceptibility.

The nonlinear interaction in the above structure is described by a Hamiltonian $\hat{H}(t)$, which is given as a sum of every layer Hamiltonian $\hat{H}^{(l)}(t)$:

$$\hat{H}(t) = \sum_{l=1}^{3} \hat{H}^{(l)}(t), \quad (2)$$

with

$$\hat{H}^{(l)}(t)$$
$$= \varepsilon_0 \int_{\upsilon} \tilde{\chi}^{(l)}(r) : \left[E_{P,\alpha}^{(l+)}(r,t) \hat{E}_{s,\beta}^{(l-)}(r,t) \hat{E}_{i,\gamma}^{(l-)}(r,t) + \text{H.c.} \right].$$
$$(3)$$

Where ε_0 is the permittivity of the vacuum and $\tilde{\chi}^{(l)}(\mathbf{r})$ represent the second-order susceptibility tensor in the lth layer. Here $l = 1,2,3$ are the marks of three layers in the cavity, the left and right regions of the cavity are marked by $l = 0$ and $l = 4$, respectively. $\widehat{E}_{p,\alpha}^{(l+)}(\mathbf{r},t)$ is the positive frequency electric field for the pump and $\widehat{E}_{m,\alpha}^{(l-)}(\mathbf{r},t)$ is the corresponding electric field operator for the generated photon with negative-frequency ω_m ($m = s,i$) in the lth layer. Here α, β, and γ denote the polarization directions [transverse electric polarization (TE) and transverse magnetic polarization (TM)]. H.c. stands for a Hermitian conjugated term.

Considering a monochromatic pump field, $E_{p,\alpha}^{(l+)}(r,t)$ in the lth layer can be written as

$$
\begin{aligned}
E_{p,\alpha}^{(l+)}(r,t) = {} & \left\{ A_{pF,\alpha}^{(l)} \exp\left[i\beta_p^{(l)}(z-z_{l-1}) \right] e_{pF,\alpha}^{(l)} \right. \\
& + \left. A_{pB,\alpha}^{(l)} \exp\left[-i\beta_p^{(l)}(z-z_{l-1}) e_{pF,\alpha}^{(l)} \right] \right\} \\
& \times \exp(i k_{p\perp} r_\perp) \exp(-i\omega_p t),
\end{aligned}
$$

$$
\alpha = \text{TE,TM}, \quad l = 0,1,2,3,4, \qquad (4)
$$

with

$$
\beta_p^{(l)} = \sqrt{\left(k_p^{(l)}\right)^2 - k_{p\perp}^2} \quad \left(k_p^{(l)} = n^{(l)}(\omega_p)\frac{\omega_p}{c} \right), \qquad (5)
$$

Where $k_p^{(l)}$ represents the wave vector of the pump field in the lth layer, $k_{p\perp}$ and $\beta_p^{(l)}$ are the transverse and longitudinal components of the wave vector. $r_\perp$ and z stand for the transverse and longitudinal coordinates, $n^{(l)}(\omega_p)$ is the refractive index for the pump field with frequency ω_p. Where $e_{pF,\alpha}^{(l)}$ and $e_{pB,\alpha}^{(l)}$ represent the unit polarization vectors for the pump field, and $A_{pF(B),\alpha}^{(l)}$ is the amplitude for the forward (backward) propagating field in the lth layer, which are determined by the boundary conditions and free fields inside the layers. The expressions for $A_{pF(B),\alpha}^{(l)}$ are given in Appendix A.

The electric-field operators $\hat{E}_{m,\alpha}^{(l-)}(r,t)$ with negative frequency for the signal and idler fields with α polarization can be described as [19]

$$
\begin{aligned}
\hat{E}_{m,\alpha}^{(l-)}(r,t) = {} & -\int_0^\infty d\omega_m \sqrt{\frac{\hbar \omega_m \zeta^{(l)}(\omega_m)}{4\pi \varepsilon_0 c \mathcal{A}} \frac{u^{(l)}(\omega_m)}{n^{(l)}(\omega_m)}} \\
& \times \left[e^{i\beta^{(l)}(z-z_{l-1})} \hat{\alpha}_{mF,\alpha}^{(l)}(\omega_m) e_{mF,\alpha}^{(l)} + e^{-i\beta^{(l)}(z-z_{l-1})} \right. \\
& \times \left. \hat{\alpha}_{mB,\alpha}^{(l)}(\omega_m) e_{mB,\alpha}^{(l)} \right] \exp(i k_{m\perp} r_\perp) \exp(i\omega_m t),
\end{aligned}
$$

$$
(6)
$$

with

$$
\zeta(\omega_m) = \frac{\varepsilon^I(\omega_m) - \kappa^I(\omega_m)|n(\omega_m)|^2}{2\gamma(\omega_m)}, \qquad (7)
$$

$$
\beta_m^{(l)} = \sqrt{\left(k_m^{(l)}\right)^2 - k_{m\perp}^2} \quad \left(k_m^{(l)} = n^{(l)}(\omega_m)\frac{\omega_m}{c} \right), \qquad (8)
$$

where ε_0 and c are the permittivity and light speed in vacuum, respectively. $\hbar$ is the reduced Planck constant, $\mathcal{A}$ denotes the area of the transverse profile of a beam. $\hat{\alpha}_{mF,\alpha}^{(l)}(\omega_m)$ and $\hat{\alpha}_{mB,\alpha}^{(l)}(\omega_m)$ are the annihilation operators for the generated field in the lth layer. $\hat{e}_{mF,\alpha}^{(l)}(\omega_m)$ and $\hat{e}_{mB,\alpha}^{(l)}(\omega_m)$ are polarization vectors of mode m of α wave propagating forward and backward with respect to the z axis. $k_{m\perp}$ is the transverse component of the wave vector, which is a constant in the whole structure. $\varepsilon^I(\omega_m)$ is the imaginary part of the electric permittivity, and $\kappa^I(\omega_m)$ is the imaginary part of the reciprocal of magnetic permittivity. $\gamma(\omega_m)$ is the imaginary part of the refractive index $n(\omega_m)$. $n^{(l)}(\omega_m)$ and $u^{(l)}(\omega_m)$ are the refractive index and magnetic permittivity for the generated field with frequency ω_m in the lth layer. The expressions for $\hat{\alpha}_{mF,\alpha}^{(l)}(\omega_m)$ and $\hat{\alpha}_{mB,\alpha}^{(l)}(\omega_m)$ are given in Appendix B.

Inserting Eqs. (4) and (6) into Eq. (2), we can get the following expression by using the transverse Fourier transformation:

$$
\begin{aligned}
\hat{H}(t) = {} & \varepsilon_0 \mathcal{A}\sqrt{2\pi} \sum_{l=1}^3 \int_{z_{l-1}}^{z_l} dz \int_0^\infty d\omega_s \\
& \times \int_0^\infty d\omega_i \tilde{\chi}^{(l)}(z) : \left\{ E_{P,\alpha}^{(l+)}(z,\omega_p) \hat{E}_{s,\beta}^{(l-)}(z,\omega_s) \right. \\
& \times \left. \hat{E}_{i,\gamma}^{(l-)}(z,\omega_i) \exp[-i(\omega_p - \omega_s - \omega_i)t] + \text{H.c.} \right\}, \\
& \alpha,\beta,\gamma = \text{TE,TM}. \qquad (9)
\end{aligned}
$$

The transverse wave vectors of the pump field and the signal and idler fields satisfy the following relation:

$$
k_{p\perp} = k_{s\perp} + k_{i\perp}. \qquad (10)
$$

Solving the Schrödinger equation to first order in nonlinear perturbation together with the assumption of incident vacuum state $|\text{vac}\rangle$, the output state $|\Psi\rangle_{s,\beta,i,\gamma}^{\text{out}}$ of signal and idler fields can be expressed as [7,8]

$$
\begin{aligned}
|\psi\rangle_{s,\beta,i,\gamma}^{\text{out}} & = \exp\left[-\frac{i}{\hbar} \int_{-\infty}^\infty dt\, H_{\text{int}}(t) \right] |\text{vac}\rangle \\
& = |\text{vac}\rangle - \frac{i}{\hbar} \lim_{T\to\infty} \int_{-T}^T dt\, \hat{H}(t) |\text{vac}\rangle. \qquad (11)
\end{aligned}
$$

Inserting Eqs. (4), (6), and (9) into Eq. (11), we arrive at the expression for the output state as

$$
\begin{aligned}
|\psi\rangle_{s,\beta,,i,\gamma}^{\text{out}} = {} & |\text{vac}\rangle - \frac{i\sqrt{2\pi}}{2c} \sum_{l=1}^3 \int_0^\infty d\omega_s \sqrt{\omega_s} \int_0^\infty d\omega_i \sqrt{\omega_i} \\
& \times \sum_{m=pF,pB} \sum_{n=sF,sB} \sum_{o=iF,iB} \tilde{\chi}^{(l)} : e_{m,\alpha}^{(l)} e_{n,\beta}^{(l)} e_{o,\gamma}^{(l)} \\
& \times \frac{\sqrt{\omega_s \omega_i \zeta_s^{(l)}(\omega_s) \zeta_i^{(l)}(\omega_i) u_s^{(l)}(\omega_s) u_i^{(l)}(\omega_i)}}{n_s^{(l)}(\omega_s) n_i^{(l)}(\omega_i)} \\
& \times A_{m,\alpha}^{(l)} L_l \exp\left[\frac{i}{2}\left(k_m^{(l)} - k_n^{(l)} - k_o^{(l)} \right) L_l \right] \\
& \times \sin c\left[\frac{1}{2}\left(k_m^{(l)} - k_n^{(l)} - k_o^{(l)} \right) L_l \right] \\
& \times \sigma(\omega_p - \omega_s - \omega_i) \hat{\alpha}_{n,\beta}^{(l)\dagger}(\omega_s) \hat{\alpha}_{o,\gamma}^{(l)\dagger}(\omega_i) |\text{vac}\rangle. \qquad (12)
\end{aligned}
$$

For the NIM-PIM-NIM cavity, we assume only the middle layer has a nonzero nonlinear coefficient and the absorption is neglected. Then, $|\Psi\rangle_{s,\beta,i,\gamma}^{\text{out}}$ can be expressed as

$$
\begin{aligned}
|\psi\rangle_{s,\beta,,i,\gamma}^{\text{out}} = {} & |\text{vac}\rangle - \frac{i\sqrt{2\pi}}{2c} \int_0^\infty d\omega_s \sqrt{\omega_s} \int_0^\infty d\omega_i \sqrt{\omega_i} \\
& \times \sum_{m=pF,pB} \sum_{n=sF,sB} \sum_{o=iF,iB} \tilde{\chi}^{(2)} : e_{m,\alpha}^{(2)} e_{n,\beta}^{(2)} e_{o,\gamma}^{(2)} \\
& \times \sqrt{\frac{\omega_s \omega_i}{n_s^{(2)}(\omega_s) n_i^{(2)}(\omega_i)}} \\
& \times A_{m,\alpha}^{(2)} L_2 \exp\left[\frac{i}{2}\left(k_m^{(2)} - k_n^{(2)} - k_o^{(2)} \right) L_2 \right]
\end{aligned}
$$

$$\times \sin c \left[\frac{1}{2} \left(k_m^{(2)} - k_n^{(2)} - k_o^{(2)} \right) L_2 \right]$$
$$\times \sigma(\omega_p - \omega_s - \omega_i) \hat{a}_{n,\beta}^{(2)+}(\omega_s) \hat{a}_{o,\gamma}^{(2)+}(\omega_i) |\text{vac}\rangle. \tag{13}$$

We are interested only in the second term of $|\Psi\rangle_{s,\beta,i,\gamma}^{\text{out}}$, the vacuum state $|\text{vac}\rangle$ can be neglected. By using the matrix-transfer formalism in Eqs. (A5) and (B2), the operators $\hat{a}_{mF,\alpha}^{(2)}$ and $\hat{a}_{mB,\alpha}^{(2)}$ can be expressed in terms of the operators $\hat{a}_{mF,\alpha}^{(4)}$ and $\hat{a}_{mB,\alpha}^{(0)}$, and the pump-field amplitudes $A_{pF,\alpha}^{(2)}(\omega_p)$ and $A_{pB,\alpha}^{(2)}(\omega_p)$ can be determined from the amplitudes of the incident fields $A_{pF,\alpha}^{(0)}$ and $A_{pB,\alpha}^{(4)}$. $A_{pB,\alpha}^{(4)}$ can be assumed to be zero. The second term $(|\Psi\rangle_{s,\beta,i,\gamma}^{(2)})$ in $|\Psi\rangle_{s,\beta,i,\gamma}^{\text{out}}$ can be decomposed into the following four parts [7,8]:

$$|\psi\rangle_{s,\beta,i,\gamma}^{(2)} = |\psi_{s,\beta,i,\gamma}^{FF}\rangle + |\psi_{s,\beta,i,\gamma}^{FB}\rangle + |\psi_{s,\beta,i,\gamma}^{BF}\rangle + |\psi_{s,\beta,i,\gamma}^{BB}\rangle, \tag{14}$$

where

$$|\psi_{s,\beta,i,\gamma}^{FF}\rangle = \int_0^\infty d\omega_s \int_0^\infty d\omega_i \big[\phi^{FF}(\omega_s,\omega_i) \hat{a}_{sF,\beta}^{(4)+}(\omega_s)$$
$$\times \hat{a}_{iF,\gamma}^{(4)+}(\omega_i) \big] |\text{vac}\rangle,$$

$$|\psi_{s,\beta,i,\gamma}^{FB}\rangle = \int_0^\infty d\omega_s \int_0^\infty d\omega_i \big[\phi^{FB}(\omega_s,\omega_i) \hat{a}_{sF,\beta}^{(4)+}(\omega_s)$$
$$\times \hat{a}_{iB,\gamma}^{(0)+}(\omega_i) \big] |\text{vac}\rangle, \tag{15}$$

$$|\psi_{s,\beta,i,\gamma}^{BF}\rangle = \int_0^\infty d\omega_s \int_0^\infty d\omega_i \big[\phi^{BF}(\omega_s,\omega_i) \hat{a}_{sB,\beta}^{(0)+}(\omega_s)$$
$$\times \hat{a}_{iF,\gamma}^{(4)+}(\omega_i) \big] |\text{vac}\rangle,$$

$$|\psi_{s,\beta,i,\gamma}^{BB}\rangle = \int_0^\infty d\omega_s \int_0^\infty d\omega_i \big[\phi^{BB}(\omega_s,\omega_i) \hat{a}_{sB,\beta}^{(0)+}(\omega_s)$$
$$\times \hat{a}_{iB,\gamma}^{(0)+}(\omega_i) \big] |\text{vac}\rangle,$$

with

$$\phi^{FF}(\omega_s,\omega_i) = -\frac{i\sqrt{2\pi}}{2c} \sum_{\substack{c=11(n=sF) \\ c=21(n=sB)}} \sum_{\substack{d=11(o=iF) \\ d=21(o=iB)}} \Gamma_{n,o} \big(R_{s,\beta}^{(2)} \big)_c (\omega_m)$$
$$\times \big(R_{i,\gamma}^{(2)} \big)_d (\omega_m) \sigma(\omega_p - \omega_s - \omega_i),$$

$$\phi^{FB}(\omega_s,\omega_i) = -\frac{i\sqrt{2\pi}}{2c} \sum_{\substack{c=11(n=sF) \\ c=21(n=sB)}} \sum_{\substack{d=12(o=iF) \\ d=22(o=iB)}} \Gamma_{n,o} \big(R_{s,\beta}^{(2)} \big)_c (\omega_m)$$
$$\times \big(R_{i,\gamma}^{(2)} \big)_d (\omega_m) \sigma(\omega_p - \omega_s - \omega_i),$$

$$\phi^{BF}(\omega_s,\omega_i) = -\frac{i\sqrt{2\pi}}{2c} \sum_{\substack{c=12(n=sF) \\ c=22(n=sB))}} \sum_{\substack{d=11(o=iF) \\ d=21(o=iB)}} \Gamma_{n,o} \big(R_{s,\beta}^{(2)} \big)_c (\omega_m)$$
$$\times \big(R_{i,\gamma}^{(2)} \big)_d (\omega_m) \sigma(\omega_p - \omega_s - \omega_i),$$

$$\phi^{BB}(\omega_s,\omega_i) = -\frac{i\sqrt{2\pi}}{2c} \sum_{\substack{c=12(n=sF) \\ c=22(n=sB)}} \sum_{\substack{d=12(o=iF) \\ d=22(o=iB)}} \Gamma_{n,o} \big(R_{s,\beta}^{(2)} \big)_c (\omega_m)$$
$$\times \big(R_{i,\gamma}^{(2)} \big)_d (\omega_m) \sigma(\omega_p - \omega_s - \omega_i), \tag{16}$$

and

$$\Gamma_{n,o} = \sum_{\substack{b=11(m=pF) \\ b=21(m=pB)}} \tilde{\chi}^{(2)} : e_{m,\alpha}^{(2)} e_{n,\beta}^{(2)} e_{o,\gamma}^{(2)} \sqrt{\frac{\omega_s \omega_i}{n_s^{(2)}(\omega_s) n_i^{(2)}(\omega_i)}} \big(R_{p,\alpha}^{(2)} \big)_b$$
$$\times (\omega_p) A_{pF,\alpha}^{(0)}(\omega_p) L_2 \exp\left[\frac{i}{2} \left(k_m^{(2)} - k_n^{(2)} - k_o^{(2)} \right) L_2 \right]$$
$$\times \sin c \left[\frac{1}{2} \left(k_m^{(2)} - k_n^{(2)} - k_o^{(2)} \right) L_2 \right], \tag{17}$$

where $\phi^{FF}(\omega_s,\omega_i)$ denotes the probability amplitude that a photon pair occurs in modes signal-forward and idler-forward, $\phi^{FB}(\omega_s,\omega_i)$ correspond to signal-forward and idler-backward, $\phi^{BF}(\omega_s,\omega_i)$ to signal-backward and idler-forward, and $\phi^{BB}(\omega_s,\omega_i)$ to signal-backward and idler-backward. Here the symbols FF, FB, BF, and BB represent the marks for four kinds of mode, respectively. The concrete forms for the matrix element $(Fp_\alpha^{(2)})_b(\omega_p)$, $(Fs_\beta^{(2)})_c(\omega_s)$, and $(Fi_\gamma^{(2)})_d(\omega_i)$ are given in the Appendixes A and B. Then $|\phi^{hk}(\omega_s,\omega_i)|^2 (h = F,B, k = F,B)$ can be expressed as

$$|\phi^{hk}(\omega_s,\omega_i)|^2 = \lim_{T\to\infty} \frac{2T}{2\pi} f(\omega_s,\omega_i) \delta(\omega_p - \omega_s - \omega_i), \tag{18}$$

with

$$f(\omega_s,\omega_i) = \frac{\pi}{c^2} |\varphi|^2, \tag{19}$$

and

$$\varphi = \sum_{\substack{c=hp(n=sF) \\ c=hq(n=sB)}} \sum_{\substack{d=kp(o=iF) \\ d=kq(o=iB)}} \Gamma_{n,o} \big(R_{s,\beta}^{(2)} \big)_c (\omega_m) \big(R_{i,\gamma}^{(2)} \big)_d (\omega_m),$$
$$Fp = 11, \quad Fq = 21; \quad Bp = 12, \quad Bq = 22, \tag{20}$$

where the period of nonlinear interaction goes from $-T$ to T. The expressions for the above physical quantities must be normalized by $2T$, which indicates that $\frac{2T}{2\pi}$ will be replaced by $\frac{1}{2\pi}$ in the calculation.

After the output states are obtained, the generation rate of correlated photon pairs can be analyzed. Thus, we define a quantity $N_{s,i}^{hk}(\omega_s,\omega_i)$ which describes the number of photon pairs that have a signal photon at the frequency ω_s and its twin idler photon at the frequency ω_i in mode mn [8]:

$$N_{s,i}^{hk}(\omega_s,\omega_i) = \langle \psi_{s,\beta,i,\gamma}^{hk} | \hat{n}_{sh,\beta}(\omega_s) \hat{n}_{ik,\gamma}(\omega_i) | \psi_{s,\beta,i,\gamma}^{hk} \rangle, \tag{21}$$

where the density operators of photons, $\hat{n}_{sh}(\omega_s)$ and $\hat{n}_{ik}(\omega_i)$, are defined as

$$\hat{n}_{sh,\alpha}(\omega_s) = \hat{a}_{sh,\alpha}^\dagger(\omega_s) \hat{a}_{sh,\alpha}(\omega_s),$$
$$\hat{n}_{ik,\alpha}(\omega_s) = \hat{a}_{ik,\alpha}^\dagger(\omega_i) \hat{a}_{ik,\alpha}(\omega_i), \tag{22}$$

with

$$\hat{\alpha}_{mF,\alpha} = \hat{a}_{mF,\alpha}^{(4)}, \quad \hat{\alpha}_{mB,\alpha} = \hat{a}_{mB,\alpha}^{(0)}. \tag{23}$$

By using Eqs. (15) and (18), the expression for $N_{s,i}^{hk}(\omega_s,\omega_i)$ can be written as

$$N_{s,i}^{hk}(\omega_s,\omega_i) = |\phi^{hk}(\omega_s,\omega_i)|^2. \tag{24}$$

If we introduce $N_s^{hk}(\omega_s)$ to describe the number of signal photons at frequency ω_s in mode hk, it can be expressed in the following form:

$$N_s^{hk}(\omega_s) = \int_0^\infty d\omega_i |\phi^{hk}(\omega_s, \omega_i)|^2. \qquad (25)$$

Sometimes, the energy spectrum of the signal field, $S_s^{hk}(\omega_s)$, is easy to measure from the experimental view. It is related to $N_s^{hk}(\omega_s)$ which is determined by the following expression:

$$S_s^{hk}(\omega_s) = \hbar\omega_s N_s^{hk}(\omega_s) = \hbar\omega_s \int_0^\infty d\omega_i |\phi^{hk}(\omega_s, \omega_i)|^2. \qquad (26)$$

Inserting Eq. (18) into Eqs. (25) and (26), $N_s^{mn}(\omega_s)$ and $S_s^{mn}(\omega_s)$ can be expressed as

$$N_s^{hk}(\omega_s) = \frac{1}{2\pi} f(\omega_s, (\omega_p - \omega_s)), \qquad (27)$$

and

$$S_s^{hk}(\omega_s) = \frac{\hbar\omega_s}{2\pi} f(\omega_s, (\omega_p - \omega_s)). \qquad (28)$$

Based on Eqs. (27) and (28), the mean number of photon pairs and the energy spectrum of the signal field can be obtained easily by the numerical calculations.

III. NUMERICAL RESULTS AND DISCUSSION

In this section, we present numerical results for the efficiency of generating a correlated photon pair by a NIM-PIM-NIM structure. In numerical calculations, we take $\omega_{pm}/\omega_{pe} = 0.8$ and $\gamma_e/\omega_{pe} = \gamma_m/\omega_{pe} = 10^{-4}$ for the NIM layer according to Ref. [21]. The middle PIM layer is assumed to be nondispersive and nonabsorbing with refractive index $n = 1.4$ [21]. The nonlinear coefficient of the middle PIM layer is taken as $\chi^{(2)} = 10$ pm/V [21]. The linear transmission spectrum for normal incidence of TE polarized mode and the density of states (DOS) as a function of the frequency for such a structure are plotted in Figs. 1(a) and 1(b), respectively. The thicknesses of NIM and PIM layers are taken as $2.5\lambda_{pe}$ and $0.16338\lambda_{pe}$ ($\lambda_{pe} = 2\pi c/\omega_{pe}$), respectively. From the transmission spectrum, we find that a transmission resonance appears in the middle of the gap, which corresponds to the maximum value of the DOS at $\omega = 0.9\,\omega_{pe}$.

If we let a pump field with $\omega_p = 1.8\,\omega_{pe}$ and $I_p = 100\,MW/cm^2$ be incident normally on the sample, making sure the output states of the signal and idler light at the resonance frequency, highly efficient generation of correlated photon pairs can be realized. Figure 2(a) shows the energy spectrum S_s^{FF} of mode FF for generated correlated photon pairs by the NIM-PIM-NIM structure as a function of normalized frequency. Here the angle (θ_s) of emergence of the signal field is taken as $\theta_s = 0$, with θ_s defined by the relation $\sin(\theta_s) = k_{s\perp}/k_s^{(0)}$, where $k_s^{(0)}$ is the signal-field wave vector in the left background. It is seen clearly that the resonant peak appears at $2\omega_s = 1.0\omega_p$. For comparison, in Fig. 2(b) we have plotted the corresponding results by the conventional three-layer heterostructure (PIM-PIM-PIM). The middle layer and size of the PIM-PIM-PIM structure are taken the same as those in the NIM-PIM-NIM structure. The solid and dotted lines correspond to the case of the dielectric constants of the
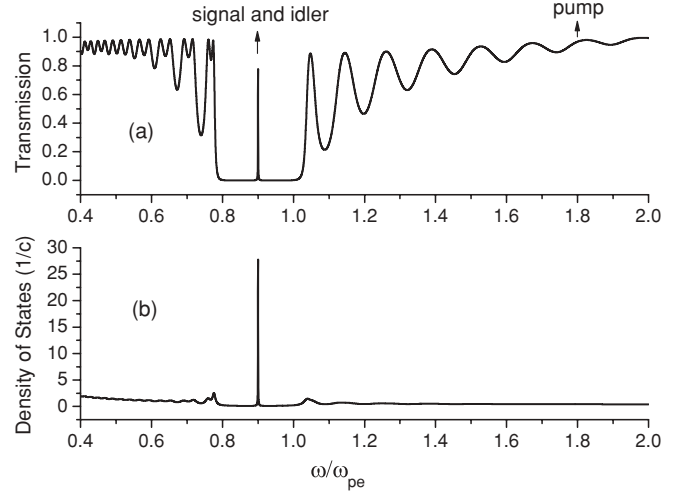
FIG. 1. Linear transmission coefficient (a) and density of states (b) as functions of the normalized frequency for the NIM-PIM-NIM structure. The thicknesses of NIM and PIM layers are taken as $2.5\lambda_{pe}$ and $0.16338\lambda_{pe}$ ($\lambda_{pe} = 2\pi c/\omega_{pe}$), respectively. $\omega_{pm}/\omega_{pe} = 0.8$, $\gamma_e/\omega_{pe} = \gamma_m/\omega_{pe} = 10^{-4}$, and the refractive index of the PIM layer is taken as 1.4.

exterior layers 3.0 and 10.0, respectively. Comparing these results with the maximum in Fig. 2(a), we find that the generation rate of correlated photon pairs can be improved by four orders of magnitude by using the NIM-PIM-NIM structure instead of the PIM-PIM-PIM structure.

Although the generation rates of correlated photon pairs in the periodically poled lithium niobate (PPLN) waveguide or fiber-based source are high [22–24], the present system also possesses some advantages in comparison with them. For example, to reach the same generation rate, we have to construct a PPLN waveguide with 200 nonlinear layers in which the thickness of each nonlinear layer is the same as the
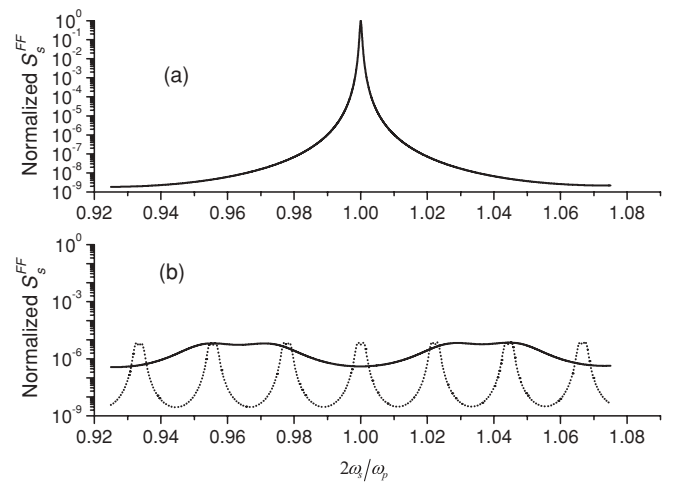
FIG. 2. Energy spectra S_s^{FF} of mode FF as a function of normalized frequency at $\omega_p = 1.8\omega_{pe}$ for the NIM-PIM-NIM structure (a) and the PIM-PIM-PIM structure (b). The parameters in the NIM-PIM-NIM structure are identical with those in Fig. 1. The middle layer in the PIM-PIM-PIM structure is the same as that in the NIM-NIM-PIM structure; the dielectric constants of the exterior layers are 3.0 (solid line) and 10.0 (dashed line).
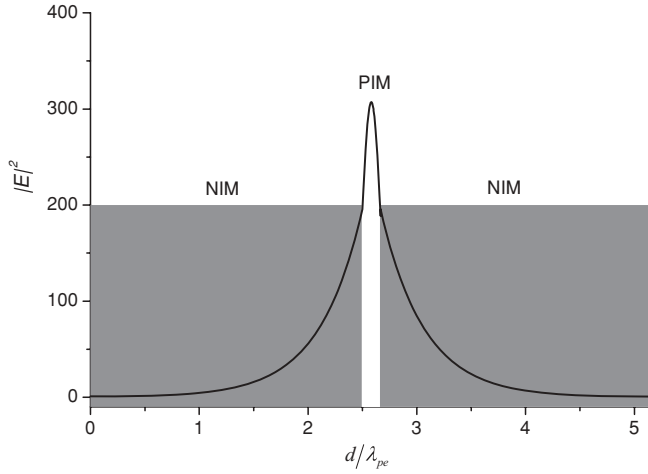
FIG. 3. Square modulus of the electric field for the NIM-PIM-NIM structure at $0.9\omega_{pe}$. The parameters are identical with those in Fig. 1.

FIG. 4. (a) Mean number of photon pairs N_s^{FF} of mode FF as a function of the thickness of the middle layer in the NIM-PIM-NIM structure at $\omega_s = 0.9\omega_{pe}$. (b) Corresponding transmission coefficient. The other parameters are identical with those in Fig. 1.

above structure; the PPLN waveguide with 100 periods only possesses one-tenth the generation rate of the present system.

The physical origin for such a highly efficient generation of correlated photon pairs can be attributed to the local resonance of the field and the quasi-phase-matching in the structure. In order to disclose such a phenomenon, in Fig. 3 we show the distribution of the electric field intensity in the structure without considering the nonlinear interaction. It is seen clearly that the field localization appears inside the sample which corresponds to the maximum of the DOS in Fig. 1(b). Thus, the nonlinear interaction can be promoted under the field localization in the nonlinear material, which leads to the improvements of the generation rate of correlated photon pairs. In fact, such a phenomenon has been observed in a defective quadratic nonlinear photonic crystal (PC) [9]. However, many-layer structures need be fabricated for the PC. The superiority of the present structure is that a three-layer system is only needed to obtain highly efficient generation of correlated photon pairs.

Furthermore, we find that the phenomenon is also sensitive to the thickness of the sample. Figure 4(a) shows the mean number of photon pairs of mode FF as a function of thickness of the middle layer in the NIM-PIM-NIM structure at $\omega_s = 0.9\omega_{pe}$. With the increase of the thickness, many resonance peaks appear, which is equivalent to the multiresonant peaks in the transmission spectrum of Fig. 4(b). This means that a high generation rate can always be obtained by tuning the thickness of the middle nonlinear layer.

The results presented above are for the case in which the output states of signal and idler photons are at the resonance frequency in the gap region while the pump field is in the band region. In fact, if the incident pump field is at the resonance frequency and the output states of signal and idler photons are in the band region, a similar phenomenon can also be observed. Figure 5(a) displays the energy spectrum of mode FF as a function of normalized frequency at $\omega_p = 0.9\omega_{pe}$ for the NIM-PIM-NIM structure. It is shown clearly that two resonance peaks at $2\omega_s/\omega_p = 0.956$ and 1.044 appear, corresponding to the output states of signal and idler photons, respectively.
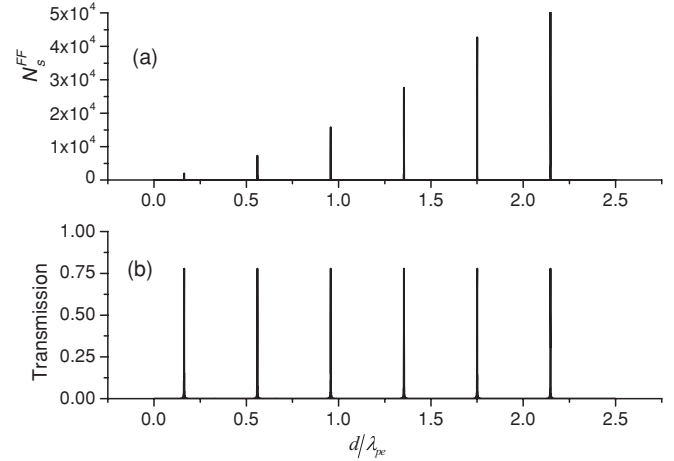
Comparing these values of S_s^{FF} with the corresponding results for the PIM-PIM-PIM structure as shown in Fig. 5(b) (solid and dashed lines correspond to the dielectric constants of the exterior layers 3.0 and 10.0, respectively), we find that the generation rate of correlated photon pairs can also be improved by three orders in the NIM-PIM-NIM structure in comparison with those in the PIM-PIM-PIM structure.

The above discussions are only for the case with $\theta_s = 0$. In fact, the generation rate of correlated photon pairs also depends on the emitted angle. Figure 6 shows the energy spectra of four kinds of mode as a function of emission angle θ_s of the signal photon for the NIM-PIM-NIM structure at
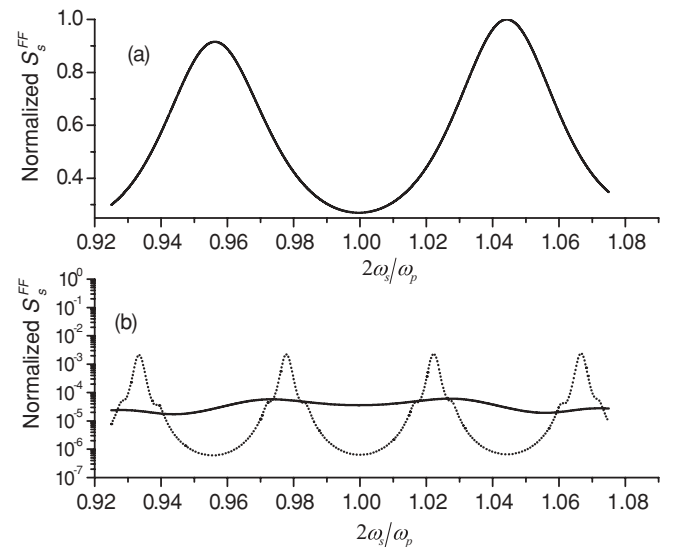
FIG. 5. Energy spectra S_s^{FF} of mode FF as a function of normalized frequency at $\omega_p = 0.9\omega_{pe}$ for the NIM-PIM-NIM structure (a) and the PIM-PIM-PIM structure (b). The parameters in the NIM-PIM-NIM structure are identical with those in Fig. 1. The middle layer in the PIM-PIM-PIM structure is the same as that in the NIM-NIM-PIM structure, the dielectric constants of the exterior layers are 3.0 (solid line) and 10.0 (dashed line).
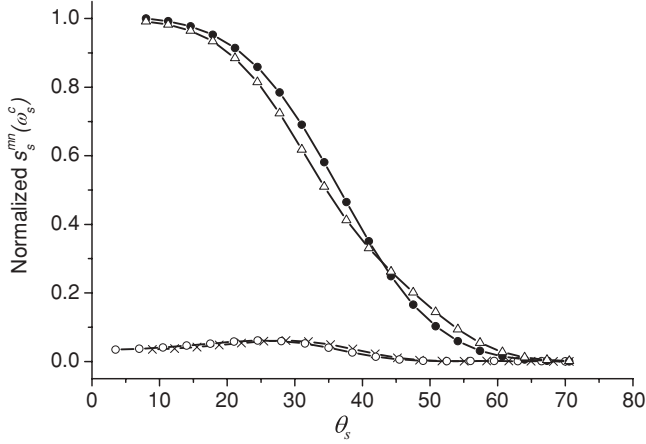
FIG. 6. Energy spectra $S_s(\omega_s)$ as a function of emission angle θ_s of the signal photon for the NIM-PIM-NIM structure at $\omega_s = \omega_p/2$ and $\omega_p = 0.9\omega_{pe}$. $\bullet$, $\triangle$, $\circ$, and $\times$ correspond to the modes FF, BB, FB, and BF, respectively. The other parameters are the same as those in Fig. 5.

$\omega_s = \omega_p/2$ and $\omega_p = 0.9\omega_{pe}$. The dark dot, triangular dot, circle dot, and cross point correspond to the modes FF, BB, FB, and BF, respectively. The generation rates of correlated photon pairs for the symmetric modes (FF and BB) are much higher than those of the nonsymmetric modes (FB and BF). The decreases also become quicker for the symmetric modes than those for the nonsymmetric modes. The decrease of the generation rate of correlated photon pairs is due to the appearance of the phase mismatching with the increase of the emission angle. This means that the phase-matching condition plays an important role in the enhancement of the correlated photon-pair generation, although the localization of the signal and idler fields in the present structure is crucial to such a process. This also means that we have to collect the output photons at the range of small angle around $\theta_s = 0$ in order to obtain a high generation rate of correlated photon pairs. In addition, we would like to point out that the above calculations only focus on the case in which the absorption and dispersion of the PIM layer are negligible. In fact, if we consider the effect of the absorption and dispersion in the PIM layer, similar phenomena can be observed except that the generation rates of correlated photon pairs decrease properly.

IV. CONCLUSION

Based on the rigorous quantum model of spontaneous parametric down-conversion, we have investigated the gen-eration efficiency of correlated photon pairs from a positive-negative index material heterostructure. We have extended the rigorous quantum theory, which has been developed for the one-dimensional dielectric photonic crystal, to the multilayer structures containing the negative index materials. The mean number of output photon pairs and the signal-field energy spectrum have been calculated. We have found that the strong confinements of both the pump and signal fields around the resonance state result in a giant enhancement of the correlated photon-pair generation. The generation rate of correlated photon pairs can be improved by several orders of magnitude in the present structure in comparison with those in the corresponding conventional system. This means that the present structure can be regarded as another alternative to be applied as a highly efficient potential source for entangled photon pairs.

APPENDIX A

In this appendix, we give the calculated method for the remaining amplitudes of the pump field $A_{pF,\alpha}^{(l)}(\omega_p)$ and $A_{pB,\alpha}^{(l)}(\omega_p)$. They are determined by the relations at the boundaries and free field inside the layers, which can be expressed as [8]

$$\begin{pmatrix} A_{pF,\alpha}^{(1)}(\omega_p) \\ A_{pB,\alpha}^{(1)}(\omega_p) \end{pmatrix} = T_{p,\alpha}^{(0)}(\omega_p) \begin{pmatrix} A_{pF,\alpha}^{(0)}(\omega_p) \\ A_{pB,\alpha}^{(0)}(\omega_p) \end{pmatrix}$$

$$\begin{pmatrix} A_{pF,\alpha}^{(l+1)}(\omega_p) \\ A_{pB,\alpha}^{(l+1)}(\omega_p) \end{pmatrix} = T_{p,\alpha}^{(l)}(\omega_p) P_p^{(l)} \begin{pmatrix} A_{pF,\alpha}^{(l)}(\omega_p) \\ A_{pB,\alpha}^{(l)}(\omega_p) \end{pmatrix} \quad \text{(A1)}$$

$$l = 1,2,3,$$

Where the symbols $A_{pF,\alpha}^{(0)}(\omega_p)$ and $A_{pB,\alpha}^{(0)}(\omega_p)$ describe the amplitudes of the pump field at the frequency ω_p incident and reflection from the left-hand side of the structure, respectively. The boundary transfer matrices, $T_{p,\mathrm{TE}}^{(l)}$ and $T_{p,\mathrm{TM}}^{(l)}$, have the form

$$T_{p,\mathrm{TE}}^{(l)} = \frac{1}{2} \begin{pmatrix} 1 + v_p^{(l)}(\omega_p)f_p^{(l)}(\omega_p) & 1 - v_p^{(l)}(\omega_p)f_p^{(l)}(\omega_p) \\ 1 - v_p^{(l)}(\omega_p)f_p^{(l)}(\omega_p) & 1 + v_p^{(l)}(\omega_p)f_p^{(l)}(\omega_p) \end{pmatrix},$$

$$T_{p,\mathrm{TM}}^{(l)} = \frac{1}{2} \begin{pmatrix} g_p^{(l)}(\omega_p) + f_p^{(l)}(\omega_p)/g_p^{(l)}(\omega_p) & g_p^{(l)}(\omega_p) - f_p^{(l)}(\omega_p)/g_p^{(l)}(\omega_p) \\ g_p^{(l)}(\omega_p) - f_p^{(l)}(\omega_p)/g_p^{(l)}(\omega_p) & g_p^{(l)}(\omega_p) + f_p^{(l)}(\omega_p)/g_p^{(l)}(\omega_p) \end{pmatrix}, \quad \text{(A2)}$$

$$l = 0,1,2,3,$$

with

$$v_p^{(l)}(\omega_p) = u_p^{(l)}(\omega_p)/u_p^{(l+1)}(\omega_p),$$
$$g_p^{(l)}(\omega_p) = n_p^{(l)}(\omega_p)/n_p^{(l+1)}(\omega_p), \quad \text{(A3)}$$
$$f_p^{(l)}(\omega_p) = \beta_p^{(l)}(\omega_p)/\beta_p^{(l+1)}(\omega_p).$$

The free-field propagation matrix is in the form

$$P_p^{(l)}(\omega_p) = \begin{pmatrix} \exp(ik_p^{(l)}L^{(l)}) & 0 \\ 0 & \exp(-ik_p^{(l)}L^{(l)}) \end{pmatrix},$$
$$l = 1,2,3. \quad \text{(A4)}$$

Furthermore, the amplitudes $A_{pF,\alpha}^{(2)}(\omega_p)$ and $A_{pB,\alpha}^{(2)}(\omega_p)$ can be expressed by $A_{pF,\alpha}^{(0)}(\omega_p)$ and $A_{pB,\alpha}^{(4)}(\omega_p)$ in the following form:

$$\begin{pmatrix} A_{pF,\alpha}^{(2)}(\omega_p) \\ A_{pB,\alpha}^{(2)}(\omega_p) \end{pmatrix} = \begin{pmatrix} (Fp_\alpha^{(2)})_{11}(\omega_p)(Fp_\alpha^{(2)})_{12}(\omega_p) \\ (Fp_\alpha^{(2)})_{21}(\omega_p)(Fp_\alpha^{(2)})_{22}(\omega_p) \end{pmatrix}$$
$$\times \begin{pmatrix} A_{pF,\alpha}^{(0)}(\omega_p) \\ A_{pB,\alpha}^{(4)}(\omega_p) \end{pmatrix}, \quad \text{(A5)}$$

where

$$Fp_\alpha^{(2)}(\omega_p)$$
$$= T_{p,\alpha}^{(1)}P_p^{(1)}(\omega_p)T_{p,\alpha}^{(0)}(\omega_p)$$
$$\times \begin{pmatrix} 1 & 0 \\ -(S_{p,\alpha})_{21}(\omega_p)/(S_{p,\alpha})_{22}(\omega_p) & 1/(S_{p,\alpha})_{22}(\omega_p) \end{pmatrix},$$
$$\text{(A6)}$$

with

$$S_{p,\alpha}(\omega_p) = T_{p,\alpha}^{(3)}(\omega_p)\prod_{l=1}^{3}\left[P_p^l(\omega_p)T_{p,\alpha}^{(l-1)}(\omega_p)\right]. \quad \text{(A7)}$$

The above expressions are obtained under the assumption of the pump field incident from the left-hand side of the cavity, so that the amplitude $A_{pB,\alpha}^{(4)}(\omega_p)$ can be taken as zero.

APPENDIX B

In this appendix we provide the expressions for the operators $\alpha_{mF}^{(l)}(\omega_m)$ and $\alpha_{mB}^{(l)}(\omega_m)$. The relation between $\hat{\alpha}_{mF,\alpha}^{(l)}(z,\omega_m)$ and $\hat{\alpha}_{mB,\alpha}^{(l)}(z,\omega_m)$ in the lth layer and $\hat{\alpha}_{mF}^{(0)}(z,\omega_m)$ and $\hat{\alpha}_{mB}^{(0)}(z,\omega_m)$ in the left-hand side of the structure can be described in the same form [19]:

$$\begin{pmatrix} \hat{\alpha}_{mF,\alpha}^{(1)}(\omega_m) \\ \hat{\alpha}_{mB,\alpha}^{(1)}(\omega_m) \end{pmatrix} = \tilde{T}_{m,\alpha}^{(0)}\begin{pmatrix} \hat{\alpha}_{mF,\alpha}^{(0)}(\omega_m) \\ \hat{\alpha}_{mB,\alpha}^{(0)}(\omega_m) \end{pmatrix},$$

$$\begin{pmatrix} \hat{\alpha}_{mF,\alpha}^{(l+1)}(\omega_m) \\ \hat{\alpha}_{mB,\alpha}^{(l+1)}(\omega_m) \end{pmatrix} = \tilde{T}_{m,\alpha}^{(l)}\tilde{P}_m^{(l)}\begin{pmatrix} \hat{\alpha}_{mF,\alpha}^{(l)}(\omega_m) \\ \hat{\alpha}_{mB,\alpha}^{(l)}(\omega_m) \end{pmatrix}, \quad \text{(B1)}$$
$$l = 1,2,3.$$

Transfer matrices $\tilde{T}_{m,\alpha}^{(l)}$ at the boundaries and free-field propagation matrices $\tilde{P}_m^{(l)}$ are defined in the same way as those given in (A2) and (A4) for the pump-field amplitudes. The operators $\hat{a}_{mF}^{(2)}(\omega_m)$ and $\hat{a}_{mB}^{(2)}(\omega_m)$ can be expressed by $\hat{a}_{mF}^{(4)}(\omega_m)$ and $\hat{a}_{mB}^{(0)}(\omega_m)$ as

$$\begin{pmatrix} \hat{\alpha}_{mF,\alpha}^{(2)}(\omega_m) \\ \hat{\alpha}_{mB,\alpha}^{(2)}(\omega_m) \end{pmatrix} = \begin{pmatrix} (Fm_\alpha^{(2)})_{11}(\omega_m)(Fm_\alpha^{(2)})_{12}(\omega_m) \\ (Fm_\alpha^{(2)})_{21}(\omega_m)(Fm_\alpha^{(2)})_{22}(\omega_m) \end{pmatrix}$$
$$\times \begin{pmatrix} \hat{\alpha}_{mF,\alpha}^{(4)}(\omega_m) \\ \hat{\alpha}_{mB,\alpha}^{(0)}(\omega_m) \end{pmatrix}, \quad \text{(B2)}$$

where

$$Fm_\alpha^{(2)}(\omega_m)$$
$$= T_{p,\alpha}^{(1)}P_m^{(1)}(\omega_m)T_{m,\alpha}^{(0)}(\omega_m)$$
$$\times \begin{pmatrix} 1/(S_{m,\alpha})_{11}(\omega_m) & -(S_{m,\alpha})_{12}(\omega_m)/(S_{m,\alpha})_{11}(\omega_m) \\ 0 & 1 \end{pmatrix}.$$
$$\text{(B3)}$$

$S_{m,\alpha}(\omega_m)$ is defined in the same way as that given in Eq. (A7).

[1] D. Bouwmeester, A. Ekert, and A. Zeilinger, *The Physics of Quantum Information* (Springer, Berlin, 2000); M. A. Nielsen and I. L. Chuang, *Quantum Computation and Quantum Information* (Cambridge University Press, Cambridge, England, 2000).

[2] E. Knill, R. Laflamme, and G. J. Milburn, Nature (London) **409**, 46 (2001).

[3] P. G. Kwiat, K. Mattle, H. Weinfurter, A. Zeilinger, A. V. Sergienko, and Y. Shih, Phys. Rev. Lett. **75**, 4337 (1995).

[4] M. J. A. de Dood, W. T. M. Irvine, and D. Bouwmeester, Phys. Rev. Lett. **93**, 040504 (2004).

[5] W. T. M. Irvine, M. J. A. de Dood, and D. Bouwmeester, Phys. Rev. A **72**, 043815 (2005).

[6] A. N. Vamivakas, Bahaa E. A. Saleh, Alexander V. Sergienko, and Malvin C. Teich, Phys. Rev. A **70**, 043810 (2004).

[7] M. Centini, J. Perina Jr., L. Sciscione, C. Sibilia, M. Scalora, M. J. Bloemer, and M. Bertolotti, Phys. Rev. A **72**, 033806 (2005).

[8] J. Perina Jr., M. Centini, C. Sibilia, M. Bertolotti, and M. Scalora, Phys. Rev. A **73**, 033823 (2006); **75**, 013805 (2007).

[9] Y. Zeng, Y. Fu, X. Chen, W. Lu, and H. Agren, J. Opt. Soc. Am. B **24**, 1365 (2007).

[10] X. Li, P. L. Voss, J. E. Sharping, and P. Kumar, Phys. Rev. Lett. **94**, 053601 (2005).

[11] J. G. Rarity, J. Fulconis, J. Duligall, W. J. Wadsworth, and P. S. Russell, Opt. Express **13**, 534 (2005).

[12] J. Fulconis, O. Alibart, W. J. Wadsworth, P. S. Russell, and J. G. Rarity, Opt. Express **13**, 7572 (2005).

[13] D. R. Smith, W. J. Padilla, D. C. Vier, S. C. Nemat-Nasser, and S. Schultz, Phys. Rev. Lett. **84**, 4184 (2000); R. A. Shelby, D. R. Smith, and S. Schultz, Science **292**, 77 (2001).

[14] C. M. Soukoulis, S. Linden, and M. Wegener, Science **315**, 47 (2007); H. O. Moser, B. D. F. Casse, O. Wilhelmi, and B. T. Saw, Phys. Rev. Lett. **94**, 063901 (2005); N. Katsarakis *et al.*, Opt. Lett. **30**, 1348 (2005).

[15] V. G. Veselago, Sov. Phys. Usp. **10**, 509 (1968).

[16] V. M. Agranovich and Y. N. Gartstein, Phys. Usp. **49**, 1029 (2006).

[17] J. B. Pendry, Phys. Rev. Lett. **85**, 3966 (2000).

[18] H. T. Dung, S. Y. Buhmann, L. Knöll, D. G. Welsch, S. Scheel, and J. Kastel, Phys. Rev. A **68**, 043816 (2003).

[19] Y. Dong and X. Zhang, Opt. Express **16**, 16950 (2008).

[20] R. W. Ziolkowski and A. D. Kipple, Phys. Rev. E **68**, 026615 (2003).

[21] N. Mattiucci, G. D'Aguanno, M. J. Bloemer, and M. Scalora, Phys. Rev. E **72**, 066612 (2005).

[22] S. Tanzilli, H. De Riedmatten, W. Tittel, H. Zbinden, P. Baldi, M. De Micheli, D. B. Ostrowsky, and N. Gisin, Electron. Lett. **37**, 26 (2001).

[23] M. Fiorentino, P. L. Voss, J. E. Sharping, and P. Kumar, IEEE Photonics Technol. Lett. **14**, 983 (2002).

[24] X. Li, J. Chen, P. Voss, J. Sharping, and P. Kumar, Opt. Express **12**, 3737 (2004).